Research Article

Received: 12 September 2023 Revised: 6 December 2023 Accepted article published: 27 December 2023 Published online in Wiley Online Library: 16 January 2024

(wileyonlinelibrary.com) DOI 10.1002/jctb.7577

Effect of large d^0 cation doping on gamma-alumina's acid–base and catalytic properties

Gabriella Garbarino,[a,b] Paola Riani,[b,c] Antonio Comite,[c] Elisabetta Finocchio[a,b*] and Guido Busca[a,b*]

Abstract

BACKGROUND: Catalysts based on alumina-supported metal oxides are of crucial importance in the field of heterogeneous catalysis for several applications requiring tuning of surface acidity.

RESULTS: In this work, the effects of K^+, Ca^{2+} and La^{3+} cation doping have been evaluated on a well-characterized commercial γ-Al_2O_3 through morphological characterization and surface characterization (Brunauer–Emmet–Teller, X-ray diffraction, field emission scanning electron microscopy, Fourier transform infrared spectroscopy). The conversion of ethanol as a test reaction was performed over these catalysts. The impregnated oxide species essentially remain at the surface, resulting in the partial poisoning of the strongest alumina Lewis acid sites. Moreover, oxide anions may increase basicity at the surface. The doping results in a significant decrease in catalytic activity in ethanol conversion to diethyl ether and to ethylene, which is shifted at higher temperatures. On the other side, higher activity in the formation of C4 olefins was detected, namely on the K-doped alumina.

CONCLUSION: The partial poisoning of the strongest alumina Lewis acid sites and the presence at the surface of new more basic cation–anion couples result in significant changes in catalytic ethanol conversion.

Keywords: alumina; modified alumina; Lewis acidity; FTIR spectroscopy

INTRODUCTION

Metal oxides are very relevant materials for many practical applications.[1] including heterogeneous catalysis.[2] Among metal oxides, gamma-alumina is a key material in the field of heterogeneous catalysis and industrial chemistry.[3,4] Its surface is characterized by strong Lewis acidic and acid–base sites, which result in strong adsorption efficiency[5] of a number of molecules. In fact, alumina, mostly in the gamma form, is used as an industrial adsorbent for drying gases and organic liquids,[6] for chlorine removal from wastes,[7] for wastewater purification such as removal of fluoride[8] and heavy metals.[9]

The strong acidity and acid–basicity of alumina are also applied industrially to catalyze important reactions[4] such as the Claus process,[10] the dehydration of alcohols to ethers[11] and olefins,[12] and some phenol alkylation reactions.[13]

On the other hand, perhaps the largest use of gamma-alumina is as a support for catalysts,[14] as in the case of many hydrogenation, dehydrogenation and oxidation metal catalysts,[15] copper chloride catalysts for oxychlorination of ethylene,[16] molybdenum and tungsten sulfide-based hydrodesulphurization catalysts,[17] etc. Gamma-alumina, due to its high density of strong acid–base sites, allows high dispersion of the supported active phases. On the other hand, as is well known,[14] industrial catalysts are usually complex materials with a large number of components besides the active phase and the support: activator and stabilizer components are usually also present to tune catalyst properties for long time-on-stream activity. In particular, alkali, alkali earth and lanthanide ions[18-20] are often added to alumina and alumina-supported catalysts to moderate acidity or to increase basicity,[21] to stabilize the catalyst against phase transformation and to modify the state of the supported phases.

The effects of cation doping are strongly affected by the cationic size of the dopant. Small cations can enter the empty sites of the defective spinel structure of gamma-alumina, thus quite easily giving rise to phase transformation and surface area loss of alumina. Instead, larger cations are not able to enter the cubic oxygen array of the spinel structure, thus generally remaining at the

* *Correspondence to: G Busca or E Finocchio, Università degli Studi di Genova, Dipartimento di Ingegneria Civile, Chimica e Ambientale (DICCA), Via all'Opera Pia 15 16145, Genoa, Italy. E-mail: guido.busca@unige.it (Busca); E-mail: elisabetta.finocchio@unige.it (Finocchio)*

a *Dipartimento di Ingegneria Civile, Chimica e Ambientale (DICCA), Università degli Studi di Genova, Genoa, Italy*

b *INSTM, UdR di Genova, Genoa, Italy*

c *Dipartimento di Chimica e Chimica Industriale (DCCI), Università degli Studi di Genova, Genoa, Italy*

external surface and stabilizing the solid. To go deeper into the effects of cation doping on γ-Al_2O_3, we undertook a study on the effect of doping gamma-alumina with large ($r > 1$ Å) d^0 ions of different charges.

Thus, we doped a commercial well-characterized material, Puralox gamma-alumina from Sasol (Hamburg, Germany), with similar molar amounts of K^+, Ca^{2+} and La^{3+}, whose ionic radius (1.38, 1.00 and 1.03 Å, respectively, for coordination 6)[22] does not allow insertion in the spinel alumina framework. To investigate the effect of doping, we used conventional infrared (IR) spectroscopic procedures and the conversion of ethanol as a test reaction. In fact, bioethanol derived from lignocellulosic materials will likely become an important chemical platform molecule in the future.[23] The conversion of bioethanol to several different secondary products is possible, thus contributing to the development of renewable industrial chemical processes.

EXPERIMENTAL

Catalysts preparation

Gamma-alumina is Puralox 200 sba produced by Sasol,[24,25] used without any further pretreatment. potassium, calcium and lanthanum ions have been introduced by wet impregnation starting from the corresponding nitrate precursors – that is, KNO_3, $Ca(NO_3)_2$ and $La(NO_3)_3.6H_2O$ – by achieving on each catalyst a final content of Al/cation mol/mol ratio of 0.012. The catalytic materials were then dried at 373 K and calcined at 823 K for 3 h. The notation is P200 for pure alumina, Ca@P200, K@P200 and La@P200 for cation-impregnated samples.

Catalyst characterization

X-ray diffraction (XRD) analyses of the fresh and exhaust catalysts were performed on an X'Pert diffractometer (CuKα radiation, Ni filter; operated in vertical mode at 40 kV and 30 mA, Philips X'Pert MPD diffractometer, The Netherlands). The diffraction patterns were recorded in the 2θ range 10–100° with a step scan mode (0.03 step width and 23 s per step). Powder patterns were indexed by comparing experimental results to the data reported in Pearson's Crystal Data database.[26]

Field emission scanning electron microscopy (FE SEM) was performed using a SUPRA 40 VP instrument (Zeiss, Jena, Germany) to investigate the sample morphology and catalyst composition, using a high sensitivity 'InLens' secondary electron detector, a solid-state backscattered electron detector and an OXFORD 'INCA Energie 450 × 3' spectrometer (Oxford Instrument, Analytical Ltd., Bucks, UK). Sample powders were directly mounted on high-purity conductive double-sided adhesive carbon tabs and then imaged.

For skeletal studies, Infrared spectra were recorded using a Thermo Nicolet 380 FTIR spectrometer (ThermoFisher Scientific, Waltam, MA, USA). The samples were pressed into thin wafers with KBr, and spectra were recorded in air (0.5 or 1 wt% sample in KBr). Spectra were collected with 100 scans (OMINC™ software, DTGS detector).

Brunauer–Emmet–Teller (BET) surface area and porosity measures were carried out using an ASAP 2020 PLUS instrument from Micromeritics (Micromeritics, Norcross, GA, USA). Before the adsorption experiment, all samples were outgassed at high vacuum and then degassed at 453 K for 4 h in a pure N_2 stream. N_2 adsorption/desorption isotherms at $0 < p/p_0 < 1$ at 77 K were experimentally obtained.

FTIR adsorption studies were performed on compacted powder disks of 15–20 mg activated in a vacuum at 773 K before adsorption experiments. Pyridine (2 torr) was put in contact with the catalysts for 10 min and then outgassed at different temperatures (423–773 K). CO_2 adsorption has been performed at room temperature (10 torr of gas in the IR cell). IR spectra of the surface have been recorded at decreasing CO_2 coverage, namely in the presence of CO_2 and after prolonged outgassing at room temperature. Ethanol (<1 torr) adsorption was performed at room temperature and upon increasing temperature under static conditions. The spectra of the catalyst surface and spectra of the gas phase were recorded at each temperature step. In all cases, a Thermo Nicolet Nexus instrument (ThermoFisher Scientific, Waltam, MA, USA) was used (OMNIC™ software, DTGS detector, 100 scans).

Catalytic experiments

Catalytic experiments were performed at atmospheric pressure in a tubular flow reactor (i.d. 6 mm) using 0.500 g catalyst (60–70 mesh sieve, thus achieving a ratio between the particle and internal reactor diameter near 25) and feeding ethanol (99.8% assay, from Sigma Aldrich, St. Louis, MO, USA) in nitrogen with 11.6 h^{-1} WHSV (weight hourly space velocity) at total flow rate 80 mL min^{-1}. The carrier gas (nitrogen) was passed through a bubbler containing ethanol maintained at a constant temperature (298 K) to obtain the desired partial pressures. The temperature in the experiment was varied stepwise from 423 to 773 K. Ethanol conversion has the usual definition:

$$X_{EtOH} = (n_{EtOH}(\text{in}) - n_{EtOH}(\text{out}))/n_{EtOH}(\text{in}) \quad (1)$$

While selectivity to product *i* is defined as follows:

$$S_i = n_i/(\nu_i(n_{EtOH}(\text{in}) - n_{EtOH}(\text{out}))) \quad (2)$$

where n_i is the number of moles of compound *i*, and ν_i is the ratio of stoichiometric reaction coefficients.

The outlet gases were analyzed using a gas chromatograph (Agilent 4890) equipped with a Varian capillary column (Molsieve 5A/Porabond Q Tandem) and thermal conductivity and flame ionization detectors in series. To identify the compounds of the outlet gases, a gas chromatograph–mass spectrometer (ThermoFisher Scientific, Waltam, MA, USA) with TG-SQC column (30 m × 0.25 mm × 0.25 µm) was used.

RESULTS AND DISCUSSION

In Table 1, BET surface area, pore volume, monolayer coverage and average pore diameters are reported for each sample. The introduction of potassium and calcium is apparently not affecting the surface area, while a negligible effect is observed both for the pore volume, decreasing from 0.46 to 0.43 $cm^3\ g^{-1}$, and for the mean pore size, decreasing from 7.8 to 7.5 nm. A different behavior is observed for lanthanum-containing catalyst, where an increase in the surface area, pore volume and mean pore size is evidenced, with values of 206 $m^2\ g^{-1}$, 0.51 $cm^3\ g^{-1}$ and 8.0 nm. These effects of lanthanum doping and the slight increase in surface area are in agreement with literature data[19,20] and with our previous study, where the catalyst was prepared by incipient wetness impregnation. In fact, in this latter work, it was evidenced how a small amount of lanthanum addition not only did not significantly reduce the catalyst surface areas, but also it stabilized

Journal of Chemical Technology and Biotechnology published by John Wiley & Sons Ltd on behalf of Society of Chemical Industry (SCI).

Table 1. Catalyst notation, cation loading, morphological data and evaluated cation monolayer

Catalyst	Theoretical cation loading (wt%)	Theoretical molar loading	Actual cation loading EDX (wt%)	Surface area ($m^2\ g^{-1}$)	Pore volume ($cm^3\ g^{-1}$)	Mean pore width (4 *V*/*A*)* (nm)	Average particle size (nm)	Calculated fraction of monolayer coverage
P200	—	—	—	198	0.46	7.8	30	—
K@P200	1.0	1.0	1.0	201	0.44	7.5	30	0.12[a]
Ca@P200	1.0	1.0	1.5	201	0.43	7.6	30	0.08[b]
La@P200	3.8	1.0	3.0	206	0.51	8.0	29	0.13[c]

*Evaluated on desorption branch – BJH equation.
[a] Considering the calculated value of 6.0 atom K nm^{-2}.
[b] Considering the calculated value of 9.1 atom Ca nm^{-2}.
[c] Considering the literature datum[27] of 5.2 atom La nm^{-2}.

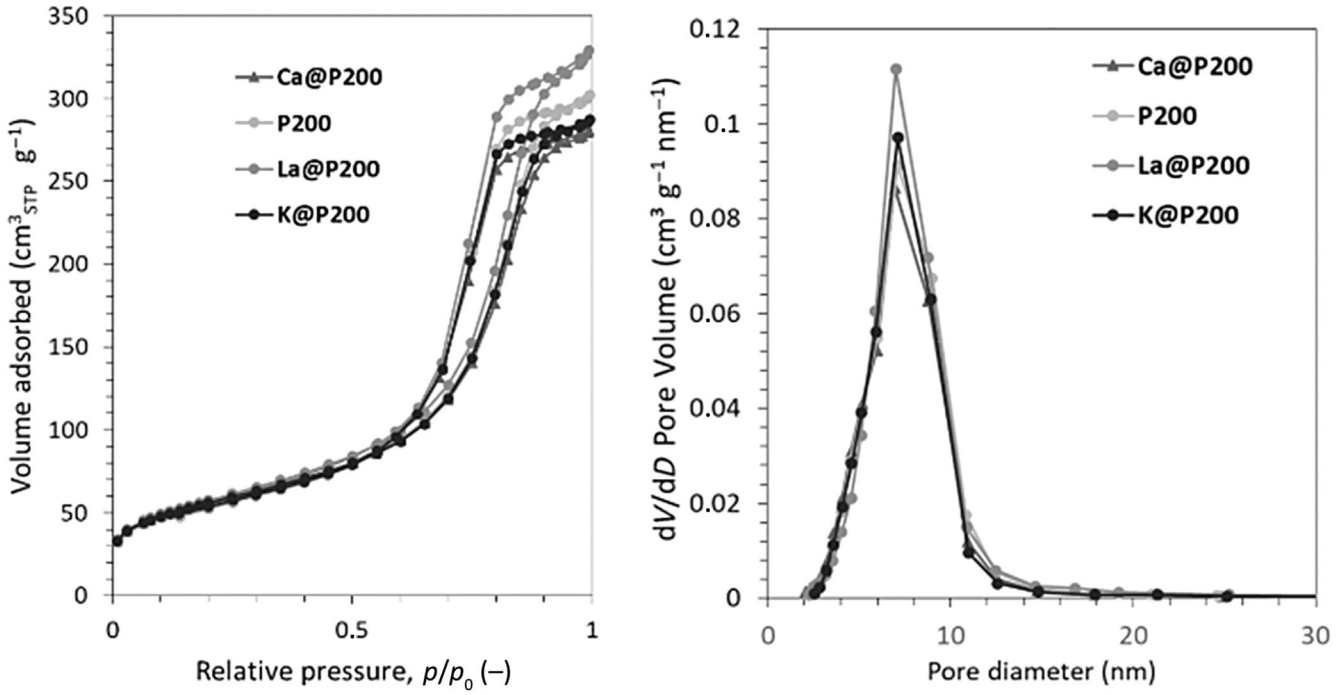

Figure 1. N_2 adsorption–desorption isotherms at 77 K (left) and pore size distribution (right) for the investigated samples.

alumina with respect to sintering, under our reaction conditions. Indeed, this effect occurred at the lowest lanthanum content, estimated to be below the nominal monolayer, while high amounts of La_2O_3 led to the formation of bulk lanthanum oxide-containing phases, lowering the catalyst surface area.[28]

In Fig. 1, N_2 adsorption–desorption isotherms and pore size distribution are reported on the left and on the right, respectively. For all the investigated catalysts, a classical IV(a) type isotherm is observed with a plateau at $p/p_0 = 0.85$ for Ca@P200, K@P200 and P200, and far higher in the case of La- modified material (La@P200), suggesting again differences in cation insertion, thus producing a material with an increased porosity of 12%. The hysteresis loops agree well with the H1 IUPAC type, identifying a parallel trend for the adsorption and desorption branches; this is typical of materials characterized by a narrow range of uniform mesopores and, apart from lanthanum-modified catalyst, no effect on pore structure is observed.[29] Pore size distribution

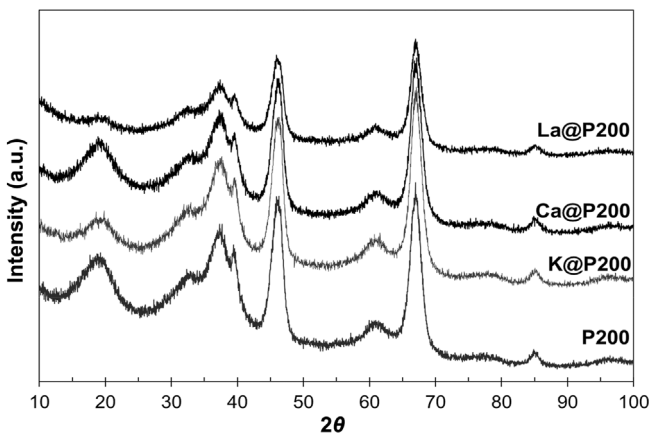

Figure 2. XRD patterns of the investigated samples as prepared. The characteristic peaks of γ-Al_2O_3 (Fe_3O_4, cF56) can be observed.

(Fig. 1, left) shows a main loss of the distribution above 10 nm when d^0 ions are impregnated onto alumina.

The experimental cation loading has been evaluated using energy-dispersive X-ray spectroscopy (EDX) spectra acquired from different regions at low magnification, and also to evaluate the homogeneity of the cation dispersion samples. The measured cation loading compares well with the theoretical one, as expected for the adopted preparation procedure.

In Fig. 2, the diffraction patterns of the synthesized catalysts are summarized. In all cases, the experimental diffraction pattern shows the characteristic peaks at 2θ 19.3 (111), 33.8 (220), 37.8 (311), 39.2 (222), 46.4 (400), 61.2 (511), 67.1 (440), 85.3 (444, 551), in good agreement with those of the reported diffraction pattern of γ-Al_2O_3 (Fe_3O_4, cF56), with typical broad features of this disordered defective spinel structure,[3,4] even though the observed features are broader than the expected ones, suggesting a more disordered arrangement in the alumina lattice. As expected, the introduction of the three cations does not significantly modify the pattern, also in agreement with their low concentration used in this case and, consequently, no evidence of peak shift is observed for the synthesized catalysts, suggesting that the cations' penetration into the bulk is in such low quantity that it cannot be observed. However, the absolute intensities of all diffraction peaks are decreased, in particular in the case of La@P200, possibly due to a surface effect, as also reported in some literature.[30]

In Fig. 3, the IR skeletal spectra of the samples in the mid-infrared region are reported. The spectra are composed of two large absorptions centered around 800 and 500 cm^{-1}, likely due to two of the four IR-active vibrational fundamental modes of spinel type structures. The other two modes are expected in the far-infrared region. The spectra are typical for γ-Al_2O_3 and are considered affected by the typical disorder of such non-stoichiometric spinel structure.[3,4] The spectrum of γ-Al_2O_3 is not significantly modified by cation doping. These data confirm that these cations do not significantly enter the alumina bulk structure. The band at 1640 cm^{-1} is due to adsorbed water. Interestingly, cation-doped samples show quite broad absorptions in the region 1600–1300 cm^{-1}, typical of surface carbonate ions. This suggests that the presence of these cations at the surface is associated with that of corresponding oxide ions, which are characterized by higher surface basicity, thus producing carbonate ions by adsorption of CO_2 from the environment.

The spectra do not show the typical sharp band of nitrate ions, centered usually around 1380 cm^{-1}. This confirms that under calcination surface nitrates were completely decomposed.

In Fig. 4, the IR spectra of the four investigated samples after activation under vacuum at 773 K in the OH stretching region are reported. The spectrum of the bare alumina P200 shows the main bands at 3766, 3726 and 3678 cm^{-1}, together with the shoulder envisaged at nearly 3785 cm^{-1}, which agrees well with features of γ-Al_2O_3 hydroxil groups reported in the literature.[3,4] Addition of the different cations introduces significant modifications in the OH group fingerprint. The main effect of lanthanum addition is some broadening and the shift down of the strongest maximum from 3725 to 3715 cm^{-1}, likely due to the formation of a new component at a slightly lower frequency, which could be due either to a perturbed AlOH or an LaOH group. This is in quite good agreement with previous data concerning slightly different samples.[31]

The addition of calcium instead results in a sharpening and shift up of the same band at 3730 cm^{-1}.

When potassium is introduced as a dopant a complete loss of the high-frequency component at 3766 cm^{-1} is observed, while a new strong component appears at 3741 cm^{-1} split from that at 3720 cm^{-1} and, at lower frequency, the band is now sharper and stronger at 3677 cm^{-1}. Also, the latter results are consistent with those obtained previously by doping fibrous alumina (Versal from UOP, Des Plaines, IL, USA) with potassium.[21]

It is relevant to note that under the conditions for recording the spectra shown in Fig. 4 weak absorptions due to residual adsorbed carbonate species are present at 1600–1200 cm^{-1} in the spectra of cation-doped aluminas, while this not the case for pure alumina.

The spectra of pyridine adsorbed over the four samples after outgassing at 300 K and 473 K are reported in Fig. 5.

As is well known, in the region reported the IR spectrum of pyridine shows four bands, denoted 8a, 8b, 19a and 19b, that in liquid pyridine are centered at 1583, 1577, 1481 and 1436 cm^{-1}, respectively[32] While the 8b and the 19a modes are almost insensitive to molecular interactions, both 8a and 19b shift up more, the stronger the interaction with a Lewis acidic cationic site.

In all cases examined, spectra of pyridine molecularly adsorbed over Lewis acid sites were observed. As usual for pyridine adsorbed on γ-Al_2O_3, after outgassing at room temperature three 8a components were observed, at 1620, 1612 and 1593 cm^{-1},

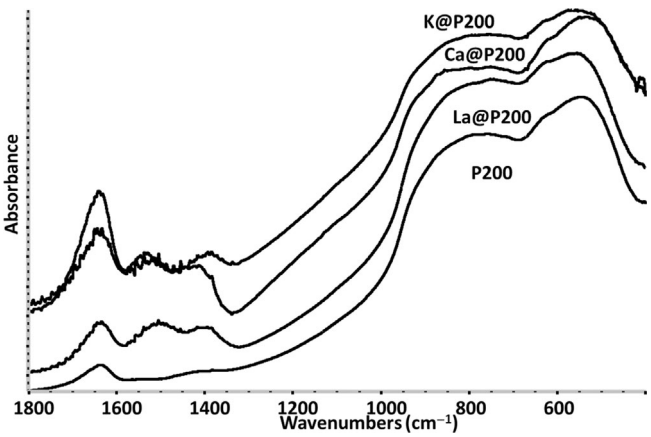

Figure 3. FTIR skeletal spectra of the investigated samples (powders diluted in KBr pressed disks).

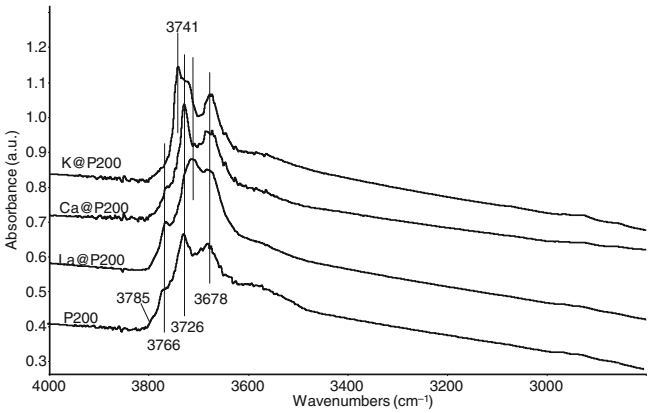

Figure 4. FTIR spectra of pure powder samples after activation under vacuum at 773 K (OH stretching region).

Journal of Chemical Technology and Biotechnology published by John Wiley & Sons Ltd on behalf of Society of Chemical Industry (SCI).

which were assigned to three different species adsorbed at three different Al^{3+} sites[5,6] with the possible presence of mono-, di- and/or tri-pyridine metal complexes.[33] Correspondingly, at least two components were found for the 19b mode at 1458 and 1447 cm^{-1}, with a possible third component around 1440 cm^{-1}. In the case of cation-doped samples, the higher-frequency components (1620 and 1458 cm^{-1}) were slightly decreased in relative intensity or fully disappeared, indicating that the strongest Lewis acid sites of alumina were decreased in amount in comparison to other Lewis sites, or disappeared. The main 8a component at 1612 cm^{-1}, likely corresponding to the 19b mode at 1447 cm^{-1}, was instead well evident in all cases, showing that medium-strength Al^{3+} Lewis acid sites were still abundant.

The third 8a mode showed different positions and strengths in the cation-doped samples. It seemed stronger in the case of La@P200, suggesting that weakly acidic Al^{3+} ions and La^{3+} ions could both contribute to the formation of this species. For Ca@P200 and K@P200, an additional component seemed to be present at 1588 cm^{-1}. In parallel, lower-frequency components were predominant or more evident also for the 19b mode, at 1443 and near 1440 cm^{-1}. These lower-frequency components could be due to pyridine species adsorbed on Ca^{2+} and K^+ ions.

After outgassing at 473 K (Fig. 5, bottom), the spectra were perturbed because of the very low intensity of the bands and the presence of weak absorptions in the original spectra of bands arising from carbonate impurities. The sensitive bands due to the 8a and 19b vibrational modes were both observed to be split at 1621, 1615 and 1460, 1450 cm^{-1} in the case of pure alumina, as is usual under these conditions.[3,4] The same doublets were also observed in the case of lanthanum- and calcium-doped samples, although the total intensity of the bands was decreased and the intensity ratio of the two components in the doublets was slightly changed in favor of the lower-frequency one. In the case of potassium-doped alumina, instead, the intensity decrease of the band was more significant and the higher-frequency component at 1621 cm^{-1} completely disappeared. Thus, in the case of potassium-doped samples, the strongest Lewis acid sites of alumina appeared to have fully disappeared. In the other cases, it seems that the density of Lewis acid sites was decreased, particularly in the case of the strongest ones. To understand these results, it must be taken into consideration that the addition of cations implies also the presence on the surface, at the end of the preparation procedure, of corresponding oxide anions. The disappearance of alumina Lewis acid sites is likely associated with their coordination saturation by oxide anions coming from impregnation and decomposition of nitrate ions.

For this reason, CO_2 adsorption and desorption were also tested over K@P200 and Ca@P200 catalysts to evidence changes in the basicity of the surface, whose Lewis acidity can be strongly affected by metal oxide doping. The corresponding IR spectra are reported in Fig. 6. Over both surfaces, after CO_2 adsorption at room temperature, the main strong bands at 1655 cm^{-1},

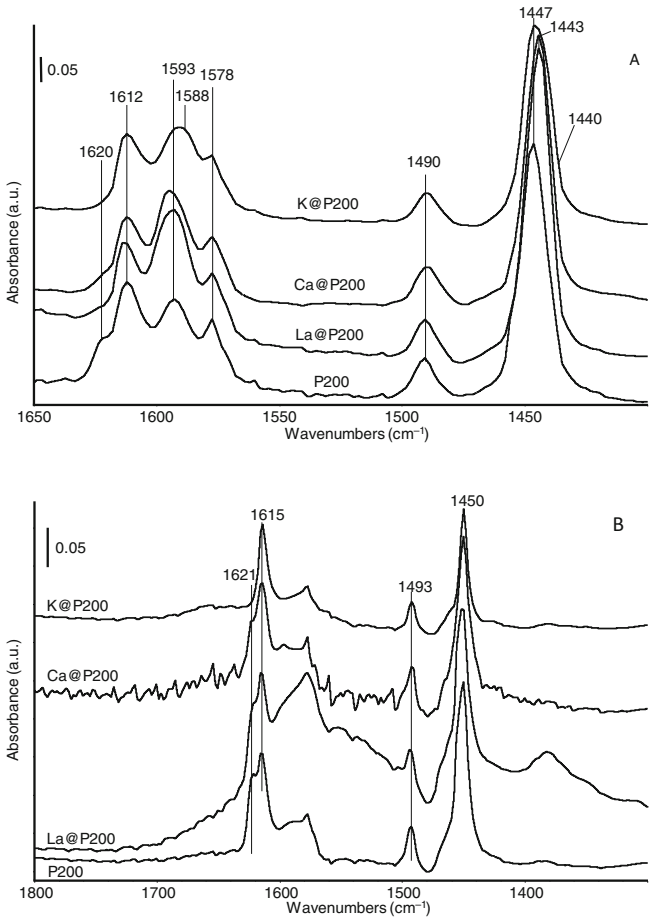

Figure 5. FTIR spectra of pyridine adsorbed over the investigated sample after previous outgassing at 773 K, adsorption at room temperature and outgassing at 300 K (A) and 473 K (B). Spectra of the catalyst are shown before adsorption has been subtracted.

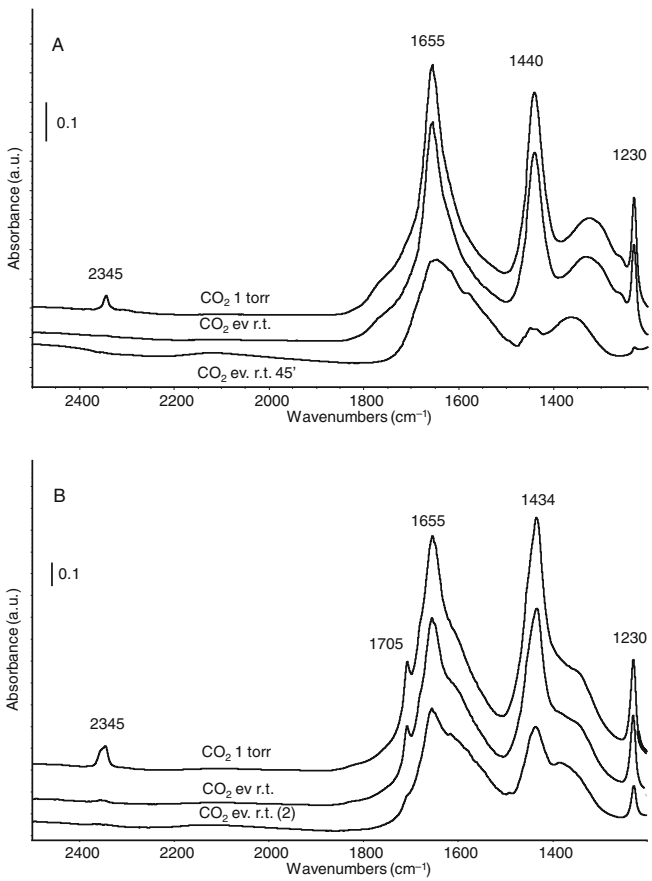

Figure 6. FTIR subtraction spectra of surface species arising from CO_2 adsorption and outgassing over K@P200 catalyst (A) and over Ca@P200 catalyst (B). The activated surface spectrum has been subtracted.

1440–1434 and 1230 cm^{-1} were ascribed to surface monohydrogen carbonate species, namely to C═O asymmetric and symmetric stretching, and OH deformation modes, respectively. Another weak absorption centered at 2345 cm^{-1} was due to molecularly adsorbed CO_2 and rapidly disappeared after outgassing.

These features are indeed consistent with results from CO_2 adsorption over pure alumina,[28] where basic (nucleophilic) hydroxyl groups are exposed at the surface, converting CO_2 into hydrogen carbonate species. Such low cation loading probably does not significantly affect the alumina surface basic sites. Moreover, the new OH groups detected after potassium loading could also be involved in hydrogen carbonate formation.

In the spectra of the K@P200 catalyst, some new components at 1320 cm^{-1} and above 1750 cm^{-1} appeared, which have been previously reported and tentatively assigned to carbonate species formation favored by potassium doping.[21]

Bicarbonate species progressively disappear after prolonged outgassing at room temperature (see the band at 1230 cm^{-1}) and new broad bands are centered at 1650, 1450 and 1360 cm^{-1}, probably due to carbonate species, suggesting the formation of new, more basic groups related to the proposed presence of potassium oxide anions. Few differences appear in the spectra of CO_2 adsorbed over the Ca@P200 sample, such as the detection of a shoulder at 1705 cm^{-1}, that almost disappears after prolonged outgassing, and two evident broad shoulders near 1600 and 1350 cm^{-1}. These features become even more evident after outgassing at 373 K and can be assigned to carbonate species in different coordinations, whose formation is enhanced by calcium doping.

The weak band of molecularly adsorbed CO_2 also shows two components: a main peak at 2345 cm^{-1}, completely consistent with the same band observed in the spectrum of the K@P200sample, together with a shoulder at higher frequencies, indicating the presence of two different adsorption sites coordinating CO_2 molecules. From these data, calcium doping also increases the surface basicity of alumina support, leading to the formation of adsorbed carbonate species that are, however, slightly different from those observed over potassium-doped catalyst.

In Fig. 7, catalytic activity results are reported in terms of ethanol conversion and selectivity to products in the temperature range 423–773 K, under steady-state conditions. Pure alumina (P200) starts to convert ethanol to ethyl ether at low temperatures (i.e., 473 K), then promptly produces ethylene with high selectivity above 623 K. Small amounts of ethane and C4 hydrocarbons are also coproduced in trace amounts. This behavior is similar to that reported in the literature for gamma-alumina tested under the same conditions.[24,28,31] Lanthanum doping shifts ethanol conversion at higher temperatures and reduces by 50% the activity observed at 473 K; however, selectivity to ethylene at high temperature (i.e., above 673 K) is comparable with those obtained over the undoped support (i.e., not far from 100%). In both cases, ethylene yield approaches 99% at 673 K.

The effect of potassium and calcium doping on catalytic performance is more relevant. In fact, over Ca@P200, ethanol starts to be

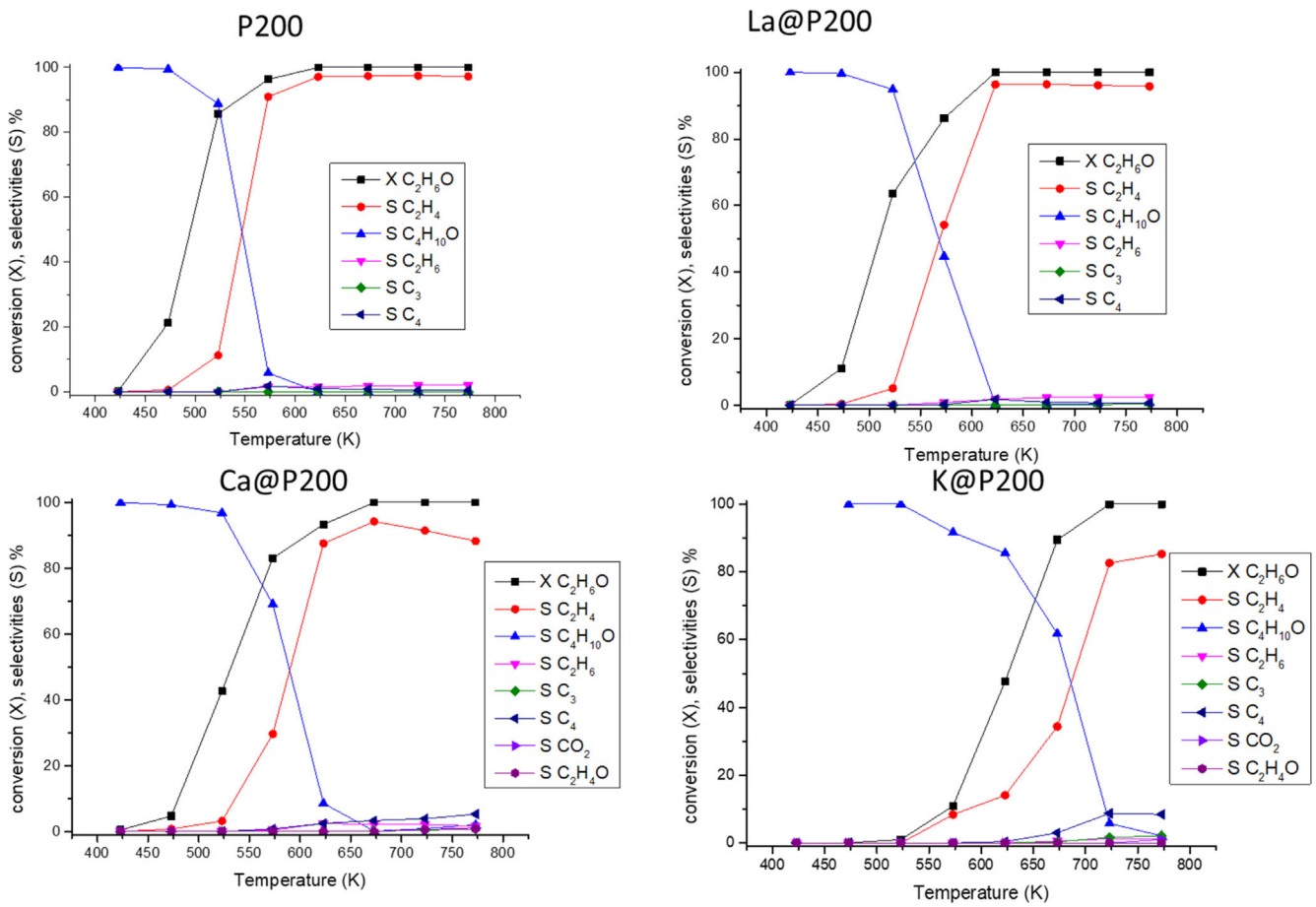

Figure 7. Ethanol conversion (X) and product selectivity (S) as a function of reaction temperature over the four catalysts.

Journal of Chemical Technology and Biotechnology published by John Wiley & Sons Ltd on behalf of Society of Chemical Industry (SCI).

converted to ethyl ether at 473 K with a reduction of 75% conversion at 523 K in comparison to pure alumina. Ethyl ether is found as the main product up to 573 K, while ethylene is found as a main by-product at higher temperatures with maximum selectivity (93%) at 673 K. C3 and C4 hydrocarbons are found in the by-product pool at $T \geq 673$ K. At 773 K, selectivity to ethylene drops below 90% for the remarkable production of C4 and C3 olefins (10% selectivity). However, the most relevant effect is again detected for potassium-doped alumina, in agreement with the characterization data presented above.

In this case, despite the low potassium loading, ethanol starts to convert only above 523 K, producing ethyl ether and ethylene at 573 K, with 90% and 10% selectivity, respectively. Ethyl ether is found as a main product up to 673 K, where C4 hydrocarbons (1,3-butadiene, 1-butene, 2-butene (both *Z*- and *E*- isomers) are also found, and whose selectivity increases upon temperature increase, resulting in a conspicuous reduction in ethylene selectivity at high *T* (80%). Catalytic activity in terms of ethanol conversion follows the order Al_2O_3 > La-Al_2O_3 > Ca-Al_2O_3 > K-Al_2O_3; while, for ethylene selectivity in the range 673–723 K, the order is Al_2O_3 ≈ La-Al_2O_3 > Ca-Al_2O_3 > K-Al_2O_3, identifying a strong effect of the dopant on catalytic performance. Interestingly, the formation of C4 hydrocarbons is enhanced by doping with calcium and, mainly, with potassium ions. This is occurring in parallel to the increased basicity of the surface and to the disappearance of strong Lewis acid sites of alumina reported in the previous paragraphs. In agreement with our data, Winkelman *et al*. suggest that a decrease in strong Lewis acid sites can be one of the reasons for the increase in butadiene formation from ethanol conversion over alkali-doped catalyst.[34] Thus, in the case of potassium-doped samples, the strongest FTIR experiments have also been performed monitoring ethanol conversion in the IR cell. Spectra of the surface species formed upon ethanol adsorption over the potassium-doped and calcium-doped samples are reported in Fig. 8 and the corresponding gas phase spectra are reported in Fig. 9. In the low-frequency region of the surface spectra, the main IR bands are centered at 1166, 1127–25 and 1073 cm^{-1} in the spectrum of the K@P200 sample and assigned, respectively, to CH_3 rocking mode (coupled with a vCO component) and to CCO stretching modes belonging to adsorbed ethoxy species. A shoulder at 1053 cm^{-1}, detected in the spectra recorded at room temperature, is assigned to H-bonded ethanol species at the catalyst surface, which disappears following heating. Correspondingly, bands assigned to hydroxyl groups and discussed in the previous paragraphs are strongly perturbed and a broad absorption in the range 3600–3500 cm^{-1} tailing towards lower frequencies confirms the presence of H-bonded undissociated ethanol (spectra not reported).

Weaker bands at 1388 cm^{-1} (sharp) and 1449–1455 cm^{-1} are attributed to CH deformation modes of the CH_3 groups, overlapped with even weaker deformation modes of the CH_2 groups.[35] Upon heating to 573 K, the bands due to ethoxy species are reduced in intensity and at 573 K carboxylate species, namely acetate species, appear, characterized by bands at 1558 and 1460 cm^{-1} (asymmetric and symmetric COO— stretching modes, respectively). A weak band at 1353 cm^{-1} can be assigned to the deformation mode of the CH_3 group. Adsorption of ethanol over the calcium sample leads to very similar results. The main bands of the spectrum are those at 1167, 1119–1117 and 1073 cm^{-1} assigned to vibrational modes of alkoxy species formed at the surface by reactive adsorption, as discussed above. In the spectrum recorded at room temperature, the presence of shoulders around

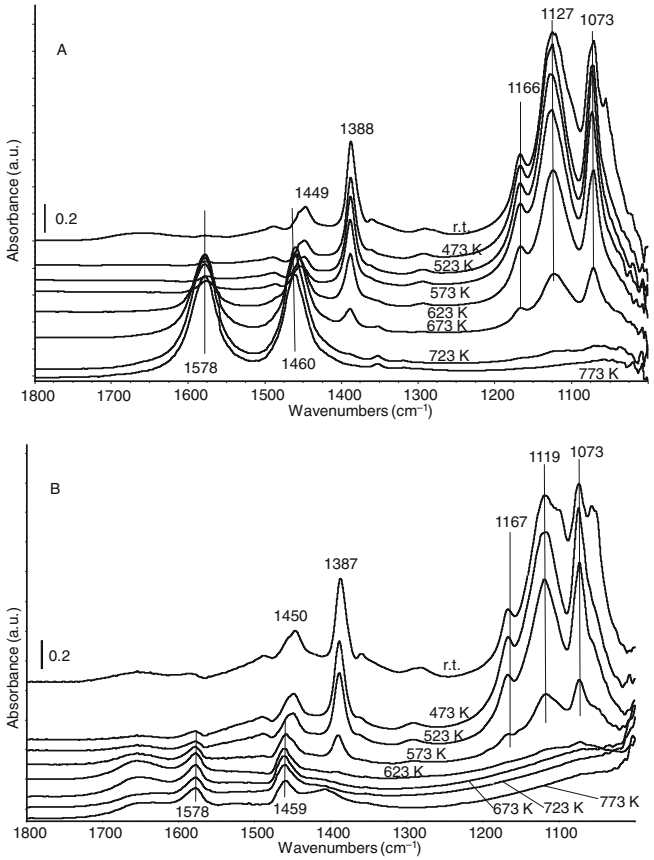

Figure 8. FTIR subtraction spectra of surface species arising from ethanol adsorption at room temperature and upon increasing temperature over K@P200 catalyst (A) and Ca@P200 catalyst (B). The activated surface spectrum has been subtracted.

1100 and 1058 cm^{-1} that disappear at increasing temperature indicates some molecularly adsorbed ethanol too. Heating leads to the decrease of these bands, which disappear between 623 and 673 K – that is, at temperatures lower than on the K@P200 catalyst. Carboxylate species, characterized by the asymmetric and symmetric stretching modes at 1578 and 1459 cm^{-1}, are formed starting from 573 K. The comparison with spectra from ethanol adsorption and thermal evolution over pure P200 alumina[35] evidenced a very similar behavior. In both cases reactive adsorption and formation of ethoxy species are predominant at the catalyst surface, as a result of the interaction with Lewis sites and some substitution of surface OH groups.

A very small amount of undissociated molecules can also be detected. Nevertheless, in the spectrum of the sample K@P200, the maximum of the broad and strong band due to asymmetric CCO stretching of adsorbed ethoxy groups is shifted up to 1125–1127 cm^{-1}; thus the frequency is slightly higher than that reported for pure alumina. This effect can suggest that potassium doping allows the formation of different ethoxy species at the surface, retaining stronger C—O bonds that might coordinate over potassium ions or bridge over aluminum and potassium ions, despite the low potassium loading of the sample. Such species are less prone to cracking, thus being stable at the surface up to 673 K, which is a significantly higher temperature than those observed under similar conditions over pure alumina. Bands assigned to OH groups at the highest frequencies disappear upon adsorption at room temperature and are progressively restored

Journal of Chemical Technology and Biotechnology published by John Wiley & Sons Ltd on behalf of Society of Chemical Industry (SCI).

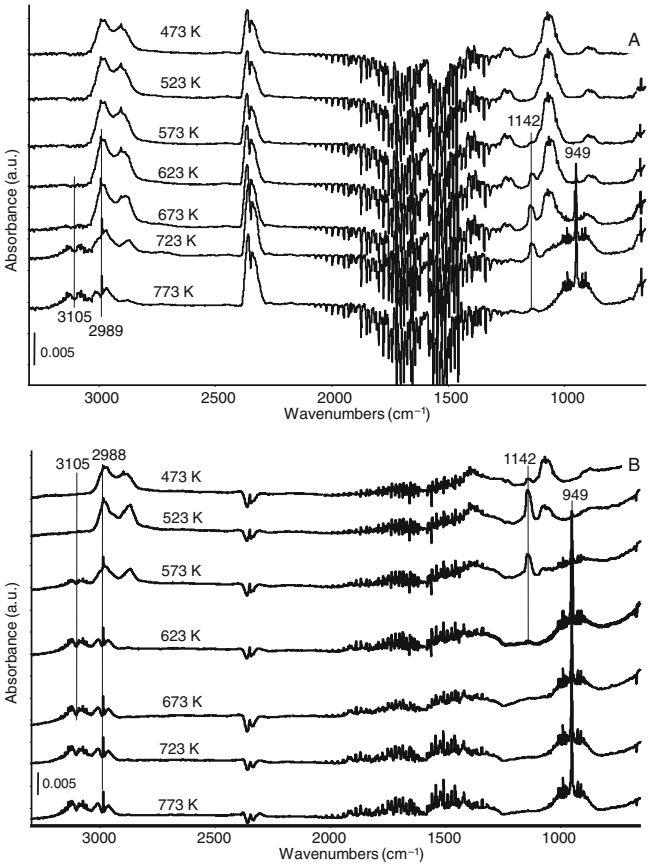

Figure 9. FTIR spectra of gas-phase species arising from ethanol adsorption upon increasing temperature over K@P200 catalyst (A) and Ca@P200 (B).

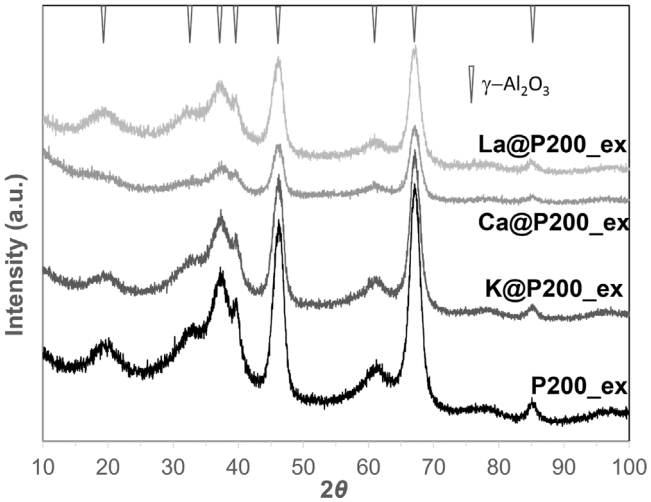

Figure 10. XRD patterns of investigated catalysts after catalytic runs, all showing only the characteristic peaks of γ-Al_2O_3 (Fe_3O_4, cF56).

after heating, in parallel with ethoxy species conversion. This effect is in agreement with results reported in previous studies on ethanol adsorption on alumina-based catalysts.[35] Also, ethanol adsorption and conversion over the calcium-doped sample show very similar behavior, through adsorbed ethoxy species, consumption of exposed OH groups, formation of carboxylate species at the highest temperatures, and final restoration of surface hydroxyls. However, the asymmetric CCO stretching is centered at wavenumbers lower than those detected for ethoxy species on K@P200 and more similar to alumina. Also, the thermal evolution of surface species evidences a decreased stability of the adsorbed alkoxy species at the Ca@P200 surface, which could be responsible for the higher reactivity of this sample in ethanol conversion at lower temperatures, in agreement with activity results.

Analysis of the gas-phase IR spectra recorded in parallel shows an initial formation of diethyl ether characterized by the COC stretching band at 1141–42 cm^{-1} for both catalysts.[36] Actually, diethyl ether is formed over the K@P200 catalyst around 573 K, and its amount peaks at 673 K, whereas on Ca@P200 diethyl ether can already be detected at 473 K, peaking at 523 K.

On the K@P200 catalyst, ethylene (bands at 949 cm^{-1} and 2989, 3105 cm^{-1}) is observed in the gas phase, starting from 623 K and rapidly becoming the predominant reaction product only above 673 K, when bands of adsorbed ethoxy groups disappear. Moreover, in the range 673–723 K, a very weak and complex band centered near 1745 cm^{-1}, together with absorption near 2700 cm^{-1}, could be assigned to the presence of a carbonyl group of aldehyde species – that is, acetaldehyde. A very similar chemistry is observed from ethanol conversion on Ca@P200, but ethylene formation is already significant at 573 K and increases up to 723 K when surface ethoxy groups completely disappear.

These results are consistent with those reported for ethanol conversion in the IR cell over pure P200 alumina, which proposed adsorbed ethoxy groups as intermediate in diethyl ether and ethylene formation, although under slightly different conditions. Over K@P200 sample the temperatures required for complete ethanol decomposition are slightly higher, indicating that doping with potassium reduced the dehydration activity of pure alumina, in agreement with ethanol conversion and selectivity found under steady-state conditions and discussed in the paragraphs above. The formation of new ethoxy groups having different coordination at the surface may explain these results.

Possibly, the presence of exposed potassium ions, having the lowest ratio charge/dimension (i.e., charge density or polarizing power) leads to a stronger interaction with alkoxides and requires an increased temperature for conversion of adsorbed species.

In this set of experiments, IR studies do not demonstrate the formation of C4 products, owing to the lower temperature range considered and to the very low partial pressure of ethanol in the IR cell, required to evidence the chemistry of adsorbed surface species.

In Fig. 10, XRD patterns of the exhaust catalysts from activity tests are reported. The diffraction patterns are similar to those of the fresh material, all revealing the characteristic peaks of γ-Al_2O_3 (Fe_3O_4, cF56), even though upon reaction a change in the relative intensity of the peaks at 2θ 19.2 and 32.9 is observable in all cases, suggesting a slight amorphization under catalytic reaction conditions. Furthermore, a strong decrease in the intensity of all the peaks in the diffraction pattern of the exhaust Ca@P200 catalyst, with respect to the fresh one, can be noticed; this may also be related to the micrographic appearance of this exhaust catalyst, observed with FE SEM, and revealing the presence of calcium-rich aggregates on the alumina surface (see Fig. 11(c,d)). The calcium-rich aggregates are amorphous; in fact, no other peaks are observed in the diffraction pattern, and their

Journal of Chemical Technology and Biotechnology published by John Wiley & Sons Ltd on behalf of Society of Chemical Industry (SCI).

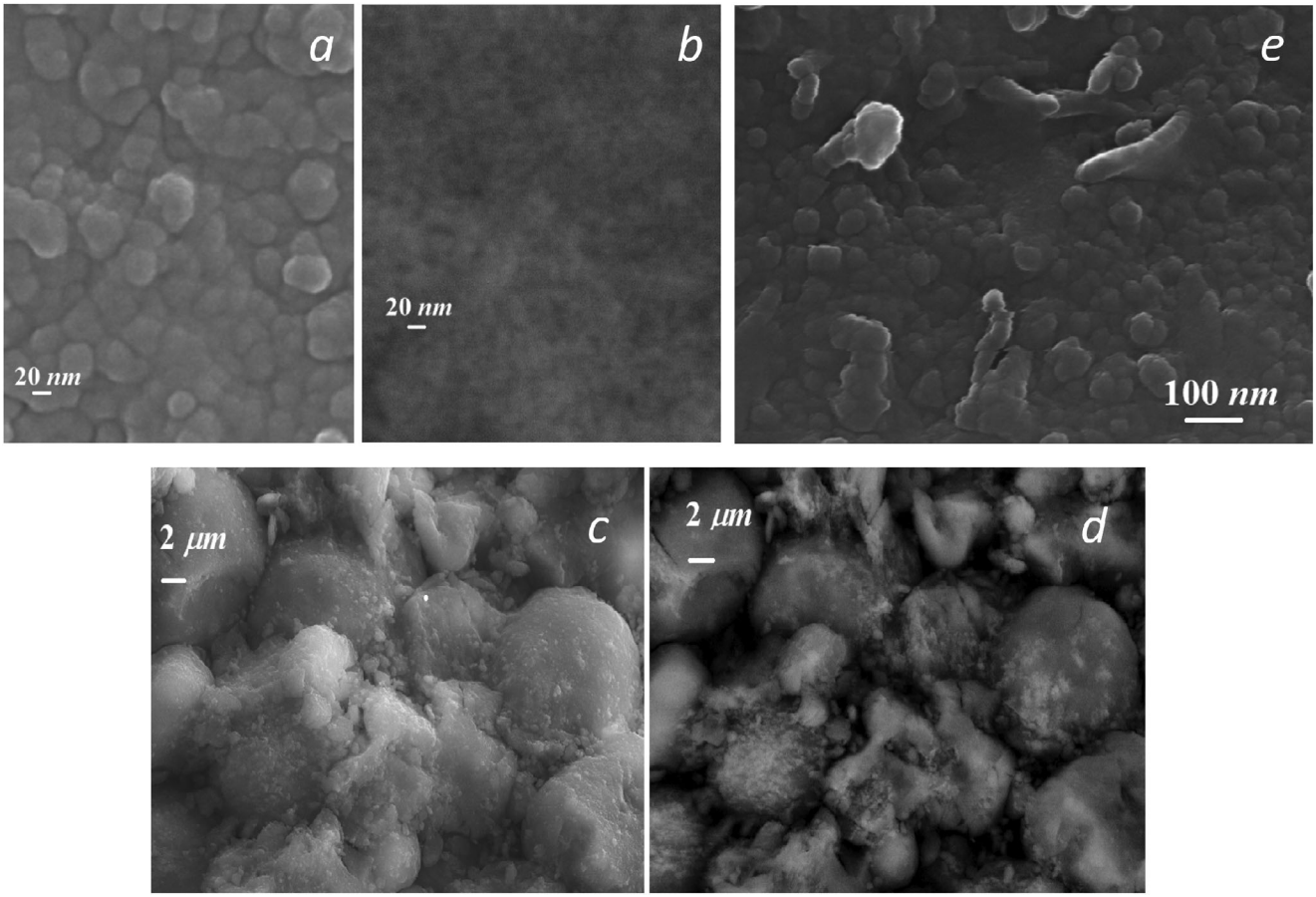

Figure 11. FE SEM micrographs of the spent catalyst, acquired using SE (insets a,e,c) and BSE (insets b,d) signals. Insets (a,b) refer to La@P200; insets (c,d) refer to Ca@P200; inset (e) refers to K@P200.

presence seems to reduce the alumina pattern intensity. Moreover, no peaks associated with carbon species are observed.

The exhausted La@P200 sample (Fig. 11(a,b)) shows small lanthanum-rich nanoparticles with a mean diameter of 5–7 nm, as observed by taking advantage of back-scattered electrons (BSE), homogeneously dispersed over the entire catalytic materials (Fig. 11(b)).

A quite different situation is observed for the Ca@P200 catalyst, where already at low magnification (Fig. 11(c,d)) calcium-rich particles are observed with an average diameter of 50–200 nm; images at high magnification allow evidence of the presence of calcium-rich particles and together the presence of calcium in the catalyst matrix. Again, a quite different situation is observed for the K@P200 catalyst, where potassium appears to be homogeneously distributed without exhibiting a change in the morphology; however, by taking advantage of secondary electrons (SE) it is possible to evidence the presence of 'worms' that can strongly resemble the presence of carbon nanotubes over the surface of the exhaust catalysts, possibly due to the higher activity evidenced in the presence of higher oligomers (see Fig. 11(e)).

CONCLUSIONS

The data reported above show that doping of gamma-alumina with moderate amounts of large d^0 cations does not result in solid-state modification of the bulk, at least if treatment temperatures do not exceed 773 K. The impregnated oxide species essentially remain at the surface. This doping results in the partial poisoning of the strongest Lewis acid sites due to highly exposed Al^{3+} ions. This is associated with the completion of their coordination by the oxide anions balancing cations. At least part of the oxide anions may, however, introduce strong basicity at the surface, as evident in particular for the potassium-doped sample. Evidence is also provided for the presence at the surface of exposed doping cations and, consequently, the formation of new OH groups likely interacting with the doping cations.

Doping results in a significant decrease of catalytic activity in ethanol conversion to diethyl ether and ethylene, which is shifted to higher temperatures, especially for the potassium-containing catalyst. Indeed, the reactive adsorption of ethanol at the surface of potassium-doped alumina probably results in more stable ethoxy species and thus less prone to cracking. Additionally, the presence at the surface of new, more basic, cation–anion couples results in new catalytic behavior, leading to some formation of C4 olefinic compounds at high temperatures.

The catalysts appear to be substantially stable after reaction, with good, stable cation dispersion. However, the deposition of carbon species is occasionally observed in the case of K@P200.

DATA AVAILABILITY STATEMENT

Data supporting the conclusion of this work are available within the article and upon reasonable request to the authors.

Journal of Chemical Technology and Biotechnology published by John Wiley & Sons Ltd on behalf of Society of Chemical Industry (SCI).

REFERENCES

1 Fierro JLG ed, *Metal Oxides: Chemistry and Applications*. CRC Press, BocaRaton, FL (2005).
2 Jackson SD and Hargreaves JSJ eds, *Metal Oxide Catalysis*. Wiley VCH, Weinheim, Germany (2009).
3 Busca G, The surface of transition aluminas. A critical review. *Catal Today* **226**:2–13 (2014).
4 Busca G, Structural, surface and catalytic properties of aluminas. *Advan Catal* **57**:319–404 (2014).
5 https://catalysts.basf.com/files/pdf/BF-9201_US_F-200_Datasheet.pdf (accessed 4th August, 2021).
6 Sircar S, Rao MB and Golden TC, Drying of gases and liquids by activated alumina. *Stud Surf Sci Catal* **99**:629–646 (1996).
7 Torres D, Jiang Y, Sanchez Monsalve DA and Leeke GA, Chlorine removal from the pyrolysis of urban polyolefinic waste in a semi-batch reactor. *J Env Che Eng* **9**:104920 (2021).
8 Wan K, Huang L, Yan J, Ma B, Huang X, Luo Z *et al*., Removal of fluoride from industrial wastewater by using different adsorbents: A review. *Sci Total Environ* **773**:145535 (2021).
9 Rahmani A, Zavvar Mousavi H and Fazli M, Effect of nanostructure alumina on adsorption of heavy metals. *Desalination* **253**:94–100 (2010).
10 https://catalysts.basf.com/files/literature-library/BASF_CAT-001731_SRU_Bruschuere_AS-viewing.pdf (accessed August 4th, 2021).
11 Tokay KC, Dogu T and Dogu G, Dimethyl ether synthesis over alumina based catalysts. *Chem Eng J* **184**:278–285 (2012).
12 Makgoba NP, Sakuneka TM, Koortzen JG, van Schalkwyk C, Botha JM and Nicolaides CP, Silication of γ-alumina catalyst during the dehydration of linear primary alcohols. *Appl Catal Gen* **297**:145–150 (2006).
13 Santacesaria E, Grasso D, Gelosa D and Carrá S, Catalytic alkylation of phenol with methanol: factors influencing activities and selectivities: I. Effect of different acid sites evaluated by studying the behaviour of the catalysts: γ-alumina, nafion-H, silica-alumina and phosphoric acid. *Appl Catal* **64**:83–99 (1990).
14 Busca G, *Heterogeneous Catalytic Materials, Solid State Chemistry, Surface Chemistry and Catalytic Behaviour*. Elsevier Publishing, Amsterdam (2014).
15 Mehrabadi BAT, Eskandari S, Khan U, White RD and Regalbuto JR, A review of preparation methods for supported metal catalysts. *Adv Catal* **61**:1–35 (2017).
16 Ohashi T, Someya S, Mori Y, Asakawa T, Hanaya M, Oguri M *et al*., Deactivation factor of CuCl2-KCl/Al2O3 catalyst for ethylene oxychlo-rination in a commercial-scale plant. *Appl Catal Gen* **589**:117205 (2020).
17 Zeelani GG, Ashrafi A, Dhakad A, Gupta G and Pal SL, A review on desulfurization techniques of liquid fuels. *Int J Sci Res* **5**:331–336 (2016).
18 Ballarini A, Basile F, Benito F, Bersani I, Fornasari G, de Miguel S *et al*., Platinum supported on alkaline and alkaline earth metal-doped alumina as catalysts for dry reforming and partial oxidation of methane. *Appl Catal Gen* **433–434**:1–11 (2012).
19 Patel K, Blair V, Douglas J, Dai Q, Liu Y, Ren S *et al*., Structural effects of lanthanide dopants on alumina. *Sci Rep* **7**:39946 (2017).
20 Wang J, Yu H, Ma Z and Zhou S, Enhanced stability of CaO and/or La2O3 promoted Pd/Al2O3 egg-shell catalysts in partial oxidation of methane to syngas. *Molecules* **18**:8289–8297 (2013).
21 Montanari T, Castoldi L, Lietti L and Busca G, Basic catalysis and catalysis assisted by basicity: FT-IR and TPD characterization of potassium-doped alumina. *Appl Catal Gen* **400**:61–69 (2011).
22 Shannon RD, Revised effective ionic radii and systematic studies of interatomic distances in halides and chalcogenides. *Acta Crystallogr* **A32**:751–767 (1976).
23 Phung TK and Busca G, Selective bioethanol conversion to chemicals and fuels via advanced catalytic approaches, in *Biorefinery of Alternative Resources: Targeting Green Fuels and Platform Chemicals, Ed by Nanda S*. Vo D-VN and Sarangi PK, Springer, Heidelberg, pp. 75–104 (2020).
24 Garbarino G, Travi I, Pani M, Carnasciali MM and Busca G, Pure vs ultrapure γ-alumina: a spectroscopic study and catalysis of ethanol conversion. *Cat Comm* **70**:77–81 (2015).
25 PURALOX, CATALOX high-purity calcined aluminas https://sasoldcproducts.blob.core.windows.net/documents/Product%20Brochures/EU_Inorganics_PURALOX%20CATALOX%20Overview.pdf (accessed Jul 8, 2021).
26 Villars P and Pearson KC, *Crystal Data: Crystal Structure Database for Inorganic Compounds (on DVD)*. ASM International®, Materials Park, OH (2020).
27 Bettman M, Chase RE, Otto K and Weber WH, Dispersion studies on the system La2O3/γAl2O3. *J Catal* **117**:447–454 (1989).
28 Garbarino G, Wang C, Valsamakis I, Chitsazan S, Riani P, Finocchio E *et al*., Acido-basicity of lanthana/alumina catalysts and their activity in ethanol conversion. *Appl Cat B: Environ* **200**:458–468 (2017).
29 Thommes M, Kaneko K, Neimark AV, Olivier JP, Rodriguez-Reinoso F, Rouquerol J *et al*., Physisorption of gases, with special reference to the evaluation of surface area and pore size distribution (IUPAC technical report). *Pure Appl Chem* **87**:1051–1069 (2015).
30 Salinas D, Escalona N, Pecchi G and Fierro JLG, Lanthanum oxide behavior in La2O3-Al2O3 and La2O3-ZrO2 catalysts with application in FAME production. *Fuel* **253**:400–408 (2019).
31 Garbarino G, Vijayakumar RPP, Riani P, Finocchio E and Busca G, Ethanol and diethyl ether catalytic conversion over commercial alumina and lanthanum-doped alumina: reaction paths, catalyst structure and coking. *Appl Catal Environ* **236**:490–500 (2018).
32 Busca G, Spectroscopic characterization of the acid properties of metal oxide catalysts. *Catal Today* **41**:191–206 (1998).
33 Busca G, Catalytic materials based on silica and alumina: structural features and generation of surface acidity. *Prog Mater Sci* **104**:215–249 (2019).
34 Winkelman AD, Lebarbier Dagle V, Lemmon TL, Kovarik L, Wang Y and Dagle RA, Effect of alkali metal addition on catalytic performance of Ag/ZrO2/SBA-16 catalyst for single-step conversion of ethanol to butadiene. *Cat Sci Technol* **13**:975–983 (2023).
35 Phung TK, Lagazzo A, Rivero Crespo MA, Sánchez Escribano V and Busca G, A study of commercial transition aluminas and of their catalytic activity in dehydration of ethanol. *J Catal* **311**:102–113 (2014).
36 Wieser H, Laidlaw WG, Krueger PJ and Fuhrer H, Vibrational spectra and a valence force field for conformers of diethyl ether and deuterated analogues. *Spectrochim Acta A* **24**:1055–1089 (1968).

Journal of Chemical Technology and Biotechnology published by John Wiley & Sons Ltd on behalf of Society of Chemical Industry (SCI).